NANO LETTERS

Ultrapure Green Light-Emitting Diodes Using Two-Dimensional Formamidinium Perovskites: Achieving Recommendation 2020 Color Coordinates

Sudhir Kumar,[†,#] Jakub Jagielski,[†,#] Nikolaos Kallikounis,[†] Young-Hoon Kim,[‡] Christoph Wolf,[§] Florian Jenny,[†] Tian Tian,[†] Corinne J. Hofer,[†] Yu-Cheng Chiu,[∥] Wendelin J. Stark,[†] Tae-Woo Lee,[‡] and Chih-Jen Shih*,[†]

[†]Institute for Chemical and Bioengineering, ETH Zürich, 8093 Zürich, Switzerland

[‡]Department of Materials Science and Engineering, Seoul National University, Seoul 08826, Korea

[§]Department of Materials Science and Engineering, Pohang University of Science and Technology (POSTECH), Pohang, Gyungbuk 790-784, Republic of Korea

[∥]Department of Chemical Engineering and Materials Science, Yuan Ze University, Taoyuan 320, Taiwan

S *Supporting Information*

ABSTRACT: Pure green light-emitting diodes (LEDs) are essential for realizing an ultrawide color gamut in next-generation displays, as is defined by the recommendation (Rec.) 2020 standard. However, because the human eye is more sensitive to the green spectral region, it is not yet possible to achieve an ultrapure green electroluminescence (EL) with a sufficiently narrow bandwidth that covers >95% of the Rec. 2020 standard in the CIE 1931 color space. Here, we demonstrate efficient, ultrapure green EL based on the colloidal two-dimensional (2D) formamidinium lead bromide (FAPbBr$_3$) hybrid perovskites. Through the dielectric quantum well (DQW) engineering, the quantum-confined 2D FAPbBr$_3$ perovskites exhibit a high exciton binding energy of 162 meV, resulting in a high photoluminescence quantum yield (PLQY) of ~92% in the spin-coated films. Our optimized LED devices show a maximum current efficiency (η_{CE}) of 13.02 cd A^{-1} and the CIE 1931 color coordinates of (0.168, 0.773). The color gamut covers 97% and 99% of the Rec. 2020 standard in the CIE 1931 and the CIE 1976 color space, respectively, representing the "greenest" LEDs ever reported. Moreover, the device shows only a ~10% roll-off in η_{CE} (11.3 cd A^{-1}) at 1000 cd m^{-2}. We further demonstrate large-area (3 cm^2) and ultraflexible (bending radius of 2 mm) LEDs based on 2D perovskites.

KEYWORDS: *Colloidal 2D perovskites, formamidinium lead bromide, dielectric quantum wells, Rec. 2020, ultrapure green, light-emitting diodes*
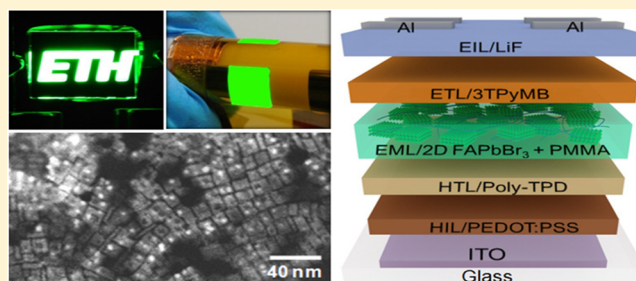
The color gamut offered by a display, which is defined the coverage in the Commission Internationale de l'Éclairage (CIE) color space, is determined by the emission properties of the pure red (R), green (G), and blue (B) light sources. The newly defined International Telecommunication Union (ITU) Recommendation BT 2020 (Rec. 2020) standard requires the monochromatic RGB primaries with extremely narrow bandwidth, which, in particular, sets a significant challenge for the green emitters. This is due to the fact that the human eye is more sensitive in the green spectral region and allows the identification of a large number of green tones.[1] The inorganic quantum dot (QD) technology have been proposed as the most promising candidate to achieve the Rec. 2020 color coordinates.[2] However, there remains two technical bottlenecks that hinder realization of the ultrapure green QD emitters: (i) a relatively wide emission bandwidth, with a full width at half-maximum (fwhm) of ~25−35 nm,[3] and (ii) a degree of

emission red shift (~5−20 nm) upon forming films from solutions.[4] Accordingly, to our knowledge, the ultrapure green electroluminescence (EL) that covers >95% of the Rec. 2020 standard in the CIE 1931 color space has never been reported by far.

Recently, the hybrid organic−inorganic lead halide perovskites are emerging as one of the most promising candidates for large-area optoelectronics because of their sizable bandgap,[5−8] solution processability,[9] and extremely long diffusion length (>μm).[10−14] Advanced photophysical analysis has revealed that the fast motion of organic cations, coupled with transient deformation of PbX$_6$ octahedral units, are responsible for the anomalously long carrier lifetime.[15,16] In consequence, the
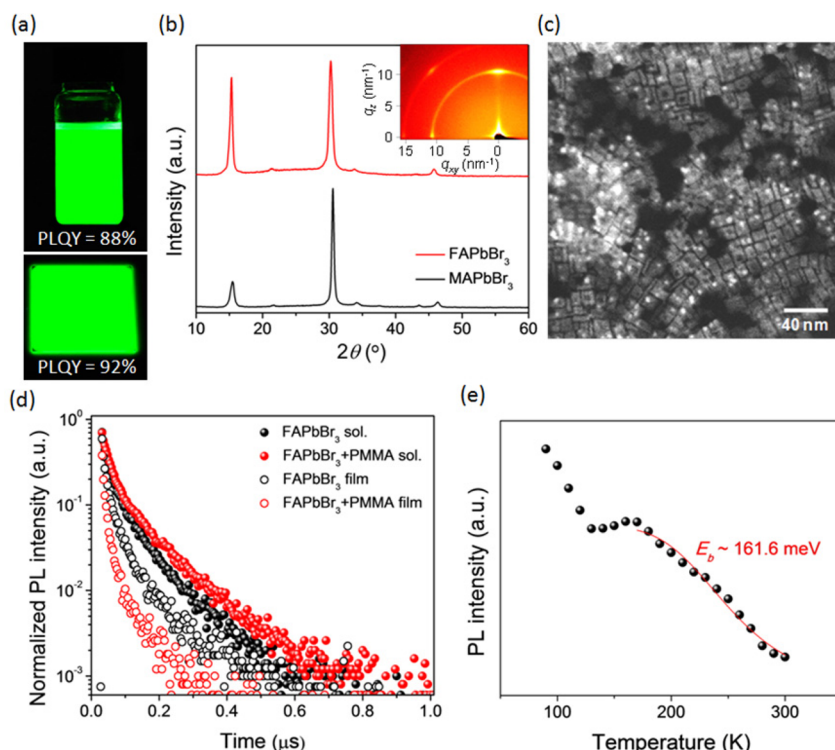
Figure 1. Characterization of 2D perovskites. (a) Photograph for the colloidal 2D $FAPbBr_3$ perovskite dispersions (top) and spin-coated coated thin film (bottom) under UV excitation. (b) XRD patterns for the thin films of the 2D $FAPbBr_3$ and $MAPbBr_3$ perovskites. Inset: GIWAXS image for the 2D $FAPbBr_3$ perovskites−PMMA complex. (c) TEM image of the 2D $FAPbBr_3$ perovskite nanoplatelets. (d) Time-resolved PL for neat 2D $FAPbBr_3$ and 2D $FAPbBr_3$−PMMA mixture in solution and in films. (e) The PL intensity for the 2D $FAPbBr_3$−PMMA complex as a function of temperature. The exciton binding energy in the cubic phase is determined to be 161.6 meV.

formation of the local ferroelectric domains[15,16] and large polarons[17] screens the Coulombic interactions between the charged carriers and the charged defects. Clearly, the fact that the hybrid perovskite systems show higher tolerance to materials defects provides a fundamental basis for the high-performance light-emitting devices.[18−21] Another practical motivation is that, compared to the inorganic QD technology, the perovskite emitters generally possess a narrower bandwidth (fwhm of ∼20−25 nm) in the green spectral range, thereby standing a better chance to approach the Rec. 2020 color coordinates. Indeed, since the first demonstration of the perovskite-based light emitting diodes (LEDs) at room temperature in 2014,[22] considerable research effort has been generated to develop the colloidal emitters with high photoluminescence quantum yields (PLQYs) and the device architectures that facilitate radiative recombination.[23−29] Nevertheless, to date, although the green perovskite LEDs with a high current efficiency (up to 42.9 cd $A^{−1}$) have been demonstrated,[13] the emission chromaticity is not sufficiently close to the Rec. 2020 standard.

A central challenge toward achieving the Rec. 2020 color coordinates with the hybrid perovskites is to precisely fine-tune the emission wavelength without sacrificing the PLQY. Specifically, considering the emission bandwidth of the hybrid perovskites, we estimate the optimal emission wavelength to be ∼525−530 nm, which is slightly lower than those for the bulk methylammonium (MA), formamidinium (FA), and cesium (Cs) lead bromide perovskites (∼540−560 nm).[30] To this end, although the chloride doping seems to be a straightforward approach to introducing a degree of blue-shifting, it often results in a drop in the PLQY (e.g., ref 31). In addition, the

solubility for the chloride precursors in the regularly used polar solvents (e.g., N,N-dimethylformamide, DMF) is low,[32] thereby increasing the process complexity in the bulk-film or nanocrystal synthesis. In this respect, the colloidal two-dimensional (2D) perovskites[33−41] might be the ultimate solution due to the following reasons. First, a precise control over the layer number enables a quantized and sizable bandgap due to the quantum confinement effect.[42] Second, the quantum confinement effect in turn enhances the exciton binding energy, E_B, which, in principle, boosts the PLQY.[30]

In this work, we demonstrate the ultrapure green LEDs based on the colloidal 2D $FAPbBr_3$ hybrid perovskites, with the stacking number of perovskite unit cells, n, to be around 7 to 10. Through the dielectric quantum well (DQW) engineering, the quantum-confined 2D $FAPbBr_3$ perovskites exhibit a high exciton-binding energy of 162 meV, resulting in a high photoluminescence quantum yield (PLQY) of 92% in the spin-coated films. Our optimized device shows a maximum current efficiency of 13.02 cd $A^{−1}$, which is among one of very few reports that reach double digits. Moreover, the EL emission locates at 529 nm with a fwhm of 22.8 nm, reaching the CIE 1931 color coordinates of (0.168, 0.773). Accordingly, for the first time, we report an ultrawide color gamut that covers 97% and 99% of the Rec. 2020 standard in the CIE 1931 and the CIE 1976 color space, respectively, representing the "greenest" LED ever reported. We further demonstrate large-area (3 cm^2) and ultraflexible (bending radius of 2 mm) LEDs based on the 2D perovskites.

The 2D $FAPbBr_3$ and $MAPbBr_3$ perovskites are synthesized by using modifications of the synthesis method developed in our previous report (for details, see the Supporting

Information).[42] In short, the first precursor, formamidinium bromide (FABr) or methylammonium bromide (MABr), was dissolved in a polar solvent, and the second precursor, lead bromide ($PbBr_2$), was dissolved in DMF. A pair of precursor solutions were next added drop-wise to a toluene solution containing two surfactants, oleic acid (OLA) and octylamine (OA). Colloidal crystallization was triggered immediately due to a low solubility of the precursors in toluene. The polar solvent used to dissolve MABr and FABr is DMF and ethanol, respectively, because the colloidal stability of 2D $FAPbBr_3$ perovskites was observed to be low at a high DMF content in toluene. The resulting precipitates were then collected and redispersed in toluene to obtain colloidal dispersions. Before device fabrication, a small amount of a low-dielectric-constant (low k) compound, poly(methyl methacrylate), PMMA, was added into the $FAPbBr_3$ colloidal solution to take advantage of DQW effect,[42] as will be discussed later.

Figure 1a presents the photograph of the 2D $FAPbBr_3$ solution and spin-coated thin film after adding PMMA under ultraviolet (UV) excitation. The PLQY of the spin-coated film composed of the 2D $FAPbBr_3$–PMMA complex is determined to be 92%, which to our knowledge, represents the highest value ever reported in the perovskite thin films. The absorption and photoluminescence (PL) spectra of 2D $MAPbBr_3$ and $FAPbBr_3$ dispersions are shown in Figure S1, with the emission wavelength, λ_{PL}, centered at 521 and 530 nm, respectively. A degree of blue-shifting, which results from the quantum confinement effect, is observed and allows us to estimate the thickness of the 2D perovskite dispersions to be $n \approx 7-10$.[42] The 2D nature of the perovskite dispersions is endorsed by the X-ray diffraction (XRD) and the transmission electron microscopy (TEM), as shown in Figures 1b,c. In the XRD spectra for both compounds, the three dominant peaks at around 15°, 30°, and 45° are assigned as the (100), (200), and (300) planes[43] for the cubic perovskite structure. The lattice constant is therefore determined to be 5.9 and 6.0 Å for 2D $MAPbBr_3$ and $FAPbBr_3$, respectively, consistent with those reported in the bulk counterparts.[44,45] Nevertheless, the peak intensity associated with other planes, such as (110) at ~21° and (210) at ~34°,[44,45] is very weak, suggesting that the crystalline symmetry possibly not be 3D. In the grazing-incidence wide-angle X-ray scattering (GIWAXS) pattern (Figures 1b inset and S2), the Debye–Scherrer ring for the (100) plane, corresponding to $q = 10.5$ nm^{-1}, becomes the strongest on the q_z axis, consistent with our previous observations in the spin-coated solids of 2D perovskite dispersions.[42]

Rectangular colloidal 2D nanocrystals were clearly identified on the TEM grids (Figures 1c and S3). In the $FAPbBr_3$ case, its emission wavelength locates at 529 ± 1 nm, corresponding to a blue shift of ~20 nm relative to that in the bulk counterpart ($n > 10$).[30] As revealed by the TEM image (Figure 1c), we observed nearly monodispersed nanocrystals with vertical and horizontal orientations, giving the average lateral length and thickness of 14.0 and 4.9 nm, respectively. Considering the unit cell thickness (~0.6 nm), $n \approx 7-10$ is therefore determined.[42] Note that the observed dark spots within the 2D structures have been suggested to be the degradation product of perovskites caused by the focused electron beam.[35] Figure S4 presents the particle size distribution (PSD) characterized using the dynamic light scattering (DLS). A narrow distribution with an average hydrodynamic diameter of 18.2 nm was observed,

confirming the colloidal monodispersity (for details, see the Supporting Information).

The concept of the dielectric confinement is realized by surrounding the 2D perovskite dispersions with a wide-bandgap, low-k compound (PMMA is used here), acting as the barrier.[42] The resulting complex consists of a matrix of the dielectric quantum wells in which the exciton binding energy is boosted due to a reduction of the effective dielectric constant.[46] Taking the 2D $FAPbBr_3$ as an example, we illustrate that the DQW engineering significantly changes the photophysical properties of the perovskite films based on the following observations: (i) an increase of PLQY from 88% (solution) to 92% (complex), as shown in Table 1; (ii) a decrease of the

Table 1. Photophysical Characteristics of 2D Perovskites-Based Solutions and Films

material	sample type	λ_{PL} (nm)	fwhm (nm)	Φ_{PLQY} (%)	τ_{avg} (ns)	E_B (meV)
$FAPbBr_3$	solution	531	21.8	88	62.7	–
	thin film	530	22.6	90	42.3	149.3
$FAPbBr_3$ + PMMA	solution	530	21.6	86	77.7	–
	thin film	530	22.6	92	24.2	161.6
$MAPbBr_3$	solution	521	23.6	79	83.8	–
	thin film	522	22.5	85	29.4	152.6

exciton lifetime (τ_{avg}) from 42.3 (neat film) to 24.2 ns (complex), as determined by the time-resolved (TR) PL spectroscopy in Figure 1d; and (iii) an increase of the exciton binding energy (E_B) from 149.3 (neat film) to 161.6 meV (complex), as determined by the temperature-dependent PL measurements in Figure 1e (for details, see the Supporting Information and Figure S5). Clearly, compared with the bulk hybrid perovskites, in which the E_B and the thermal energy at room temperature (~25 meV) are in the same order of magnitude,[47] the synthesized 2D perovskites are much more excitonic, although the degree of quantum confinement is small. We therefore infer that the dielectric confinement effect, which has been proven to be long-range,[46] is responsible for the binding energy enhancement because the colloidal nanocrystals are dispersed in low-dielectric-constant media (toluene or PMMA). The orientation, packing, and self-assembly behavior of the surrounding molecules determines the effective dielectric constant of the environment, which may be worth further investigation. In principle, a lower surrounding dielectric constant leads to a higher E_B, thereby decreasing the lifetime and increasing the PLQY, which is qualitatively supported by the photophysical characteristics of our 2D $FAPbBr_3$ samples (see Table 1).

Figure 2a presents the PL spectra for the 2D $FAPbBr_3$-based solutions and films, together with the EL spectrum. For the samples considered, the emission characteristics are nearly identical, with λ_{PL} at 530 ± 1 nm and with a fwhm of 22 ± 1 nm. This finding implies that the synthesized 2D perovskites are nearly monodispersed, such that the particle aggregation or the energy-transfer (ET) pathways created upon forming films, as reflected by a reduction in the exciton lifetime (Figure 1d), only result in a negligible degree of red-shifting distinct from that observed in the inorganic QD systems.[48] In practice, the consistent emission characteristics between solutions and films are essential for the development of the ultrapure emitters with specific chromaticity. In that sense, it appears that the 2D perovskites have advantages over the inorganic QD materials.
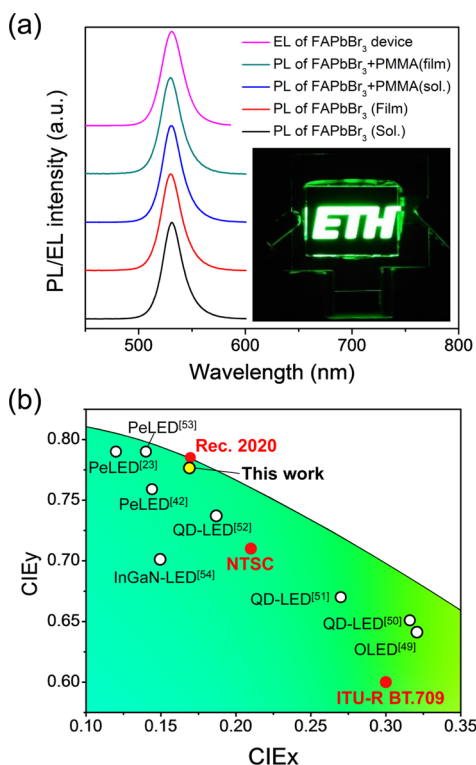
Figure 2. Basic PL and EL spectroscopic performance. (a) PL spectra for the colloidal 2D FAPbBr$_3$ perovskites in toluene solution (black), thin film (red), mixture with PMMA in toluene solution (blue), and complex with PMMA in film (green). The EL spectrum in LED device is also shown for comparison (pink). Inset: Photograph of a large-area LED device. Logo reproduced with permission. Copyright 2017 ETH Zürich, Switzerland. (b) The color coordinates of the LED device based on the 2D FAPbBr$_3$ perovskites (this work) on the CIE 1931 color space, together with the ITU-R BT.709, NTSC, and the Rec. 2020 standards, in comparison with different LED technologies, including OLED,[49] InGaN,[54] QD,[50−52] and perovskites (Pe).[23,42,53]

Table 2. Calculated Gamut Coverage Relative to Different Standards Using the Ultrapure Green LEDs Reported Here in the CIE 1931 and the CIE 1976 Color Space

	gamut area coverage/color saturation (%)	
standard	in 1931 CIEx,y	in 1976 CIE$_{u',v'}$
Rec. 2020	96.8	99.2
IBT-R BT.709	153.7	123.6
NTSC	108.9	107.8

(UPS) (for details, see the Supporting Information and Figure S6). The conduction band minimum (CBM) energy levels were then back calculated by subtracting the optical bandgap values from the PL emission wavelengths. We use a typical three-layered structure, which consists of a hole-transport layer (HTL), an emission layer (EML), and an electron-transport layer (ETL) (for molecular structures, see Figure S7). A number of experiments were carried out to optimize the HTL and ETL materials in the FAPbBr$_3$ devices, as summarized in Table 3. The control device, without PMMA in the EML (ITO/PEDOT:PSS/2D FAPbBr$_3$/TPBi/LiF/Al), shows a maximum current efficiency (η_{CE}) of 1.58 cd A^{-1} and a maximum luminance (L_{max}) of 229 cd m^{-2}, corresponding to the maximum power efficiency (η_{PE}) of 1.29 lm W^{-1} and the external quantum efficiency (η_{ext}) of 0.38%. The device based on the 2D FAPbBr$_3$−PMMA complex improves significantly. In addition to the dielectric confinement effect, we attribute the enhancement to the formation of a smoother EML (Figure S8) so that the possible electrical shunts between two transport layers are minimized. Indeed, as revealed by SEM (Figure S9), we observe rough surface and a considerable portion of uncovered patches in the spin-coated film of neat 2D FAPbBr$_3$ perovskites. On the contrary, upon mixing with PMMA, a significantly higher degree of surface coverage and smoothness is achieved, particularly on PEDOT:PSS (see more detail in section 3.4 of the Supporting Information). High performance (η_{CE} = 6.16 cd A^{-1}, η_{PE} = 4.98 lm W^{-1}, η_{ext} = 1.43%, and L_{max} = 2755 cd m^{-2}) was achieved by incorporating a thin layer of poly-TPD as the HTL after PEDOT:PSS due to a more-effective exciton confinement. We also tested two other hole-transport materials (PVK and TFB) but did not observe a substantial improvement.

Next, to further enhance the device performance, three other electron-transport materials (BPhen, B3PYMPM, and 3TPYMB) were investigated. We achieved the optimal characteristics with 3TPYMB (η_{CE} = 10.0 cd A^{-1}, η_{PE} = 7.71 lm W^{-1}, η_{ext} = 2.31%, and L_{max} = 3267 cd m^{-2}). Moreover, the device performance is markedly enhanced (η_{CE} = 13.02 cd A^{-1}, η_{PE} = 13.36 lm W^{-1}, η_{ext} = 3.04%, and L_{max} = 2939 cd m^{-2}) with the optimal emissive layer composition and charge transporting layer thicknesses (for details, see Tables 3 and S2). The device cross-sectional scanning electron micrograph is shown in Figure S10, and the performance summary of different device structures is shown in Table 3. The current efficiency reported here is among one of very few reports that have achieved double digits in colloidal nanocrystal-based perovskite LEDs (Table S3) and improves by nearly 5-fold compared with the LED devices based on the bulk FAPbBr$_3$ perovskites.[45] The current density and luminance as a function of voltage are shown in Figure 3c, and the calculated η_{CE} and η_{ext} versus current density are shown in Figure 3d (see Figure S11a for η_{PE}). In particular, the efficiency roll-off at high voltage has been significantly reduced compared with those reported in

The LED devices were then fabricated using the synthesized 2D MAPbBr$_3$ and FAPbBr$_3$, which yield EL with the emission wavelength at 524 and 529 nm, respectively. Because the color coordinates for 2D FAPbBr$_3$ are closer to the Rec. 2020 standard; thereafter, we focus on the FAPbBr$_3$-based devices. The color coordinates of the 2D FAPbBr$_3$ LED presented here (this work) in the CIE 1931 color space are shown in Figure 2b. The Rec. 2020, National Television System Committee (NTSC), and Rec. BT 709 standards are also included. Accordingly, we demonstrate an ultrapure green EL with the color coordinates of (0.168, 0.773), which, to our knowledge, represents the purest green emission ever reported, relative to the Rec. 2020 standard (0.170, 0.797). The color coordinates for other technologies, including organic LED (OLED), QD-LED, InGaN LED, and perovskite LED (PeLED),[23,42,49−54] are also attached for comparison. Indeed, the chromaticity reported here results in an ultrawide gamut that covers 97% and 99% of the Rec. 2020 standard in the CIE 1931 and CIE 1976 color space, respectively, as summarized in Table 2, which has never been achieved in LED devices thus far.

The device architecture and energy diagram for our LED device is shown in panels a and b of Figure 3 (for details, see the Supporting Information). The energy levels of valence band maximum (VBM) for 2D FAPbBr$_3$ and MAPbBr$_3$ perovskites were obtained using the ultraviolet photoelectron spectroscopy
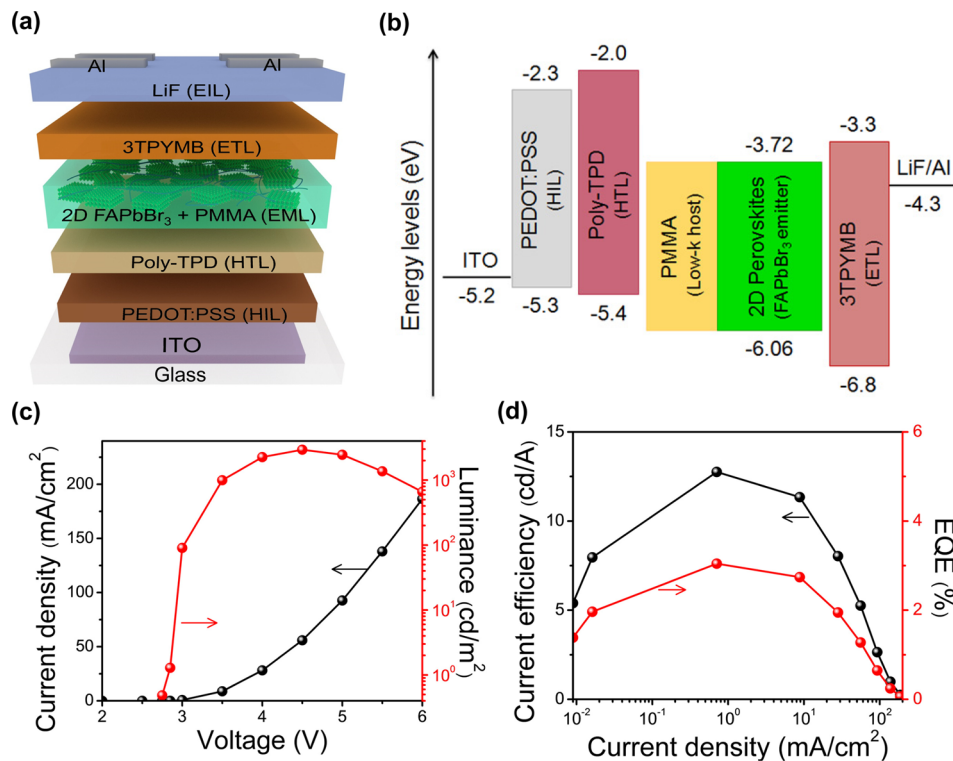
Figure 3. Device characteristics of the 2D FAPbBr$_3$ perovskite-based LEDs. (a) Schematic device architecture. (b) Energy diagram for the materials used in the optimized device. (c) Current density and luminance as a function of voltage. (d) Current efficiency and EQE as a function of current density.

Table 3. Electroluminescence Characteristics of 2D-Perovskites-Based LEDs

HTL	EML	ETL	V_{on} (V)	η_{CE} (cd A^{-1})	η_{PE} (lm W^{-1})	η_{ext} (%)	$L_{max.}$ (cd m^{-2})	λ_{EL}/fwhm (nm)
–	FAPbBr$_3$	3TPYMB (35 nm)	2.7	4.53	4.10	1.14	301	529/22.5
poly-TPD	FAPbBr$_3$	3TPYMB (35 nm)	2.8	6.46	5.80	1.57	2608	529/22.4
poly-TPD	FAPbBr$_3$ + 15 wt % PMMA	3TPYMB (35 nm)	2.8	10.00	7.71	2.31	3267	529/22.6
poly-TPD	FAPbBr$_3$ + 15 wt % PMMA	3TPYMB (35 nm)	3.0	8.22	7.38	1.99	4425	530/22.5
–	FAPbBr$_3$ + 8 wt % PMMA	3TPYMB (45 nm)	2.75	12.76	12.95	3.02	575	530/22.6
poly-TPD	FAPbBr$_3$ + 8 wt % PMMA	3TPYMB (45 nm)	2.75	13.02	13.36	3.04	2939	**529/22.8**
–	FAPbBr$_3$	TPBi (35 nm)	3.0	1.58	1.29	0.38	229	529/23.5
–	FAPbBr$_3$ + 15 wt % PMMA	TPBi (35 nm)	3.0	4.05	3.54	1.01	717	530/24.0
poly-TPD	FAPbBr$_3$	TPBi (35 nm)	3.0	2.30	1.84	0.56	1637	529/23.7
poly-TPD	FAPbBr$_3$ + 15 wt % PMMA	TPBi (35 nm)	3.0	6.16	4.98	1.43	2755	529/24.3
PVK	FAPbBr$_3$ + 15 wt % PMMA	TPBi (35 nm)	3.3	1.72	1.54	0.42	129	530/24.3
TFB	FAPbBr$_3$ + 15 wt % PMMA	TPBi (35 nm)	3.4	3.10	2.20	0.73	2511	529/23.7
poly-TPD	FAPbBr$_3$ + 15 wt % PMMA	B3PYMPM(35 nm)	3.0	2.21	2.10	0.54	1092	529/22.1
poly-TPD	FAPbBr$_3$ + 15 wt % PMMA	BPhen (35 nm)	2.6	1.28	1.15	0.31	529	530/24.3
poly-TPD	MAPbBr$_3$ + TFB	TPBi (35 nm)	3.0	2.80	2.20	0.73	2498	524/23.1
poly-TPD	MAPbBr$_3$ + TFB	3TPYMB (35 nm)	3.0	8.43	7.64	2.06	2735	524/23.5

other FAPbBr$_3$ perovskite-based LEDs, e.g., ref 55. More importantly, the optimal device only showed a ~ 10−15% roll-off in the η_{CE} (11.3 cd A^{-1}), η_{PE} (10.2 lm W^{-1}), and η_{ext} (2.74%) at 1000 cd m^{-2}. We attribute the superior device performance to a balanced charge injection and efficient exciton recombination resulting from the following mechanisms: (i) a low highest occupied molecular orbital (HOMO) level (−5.4 eV) in the poly-TPD HTL and a high lowest unoccupied molecular orbital (LUMO) level (−3.3 eV) in the 3TPYMB ETL,[56,57] thereby enabling cascade carrier injection; (ii) comparable carrier mobilities in HTL and ETL;[56,58] and (iii) an effective carrier confinement due to a high LUMO level (−2.0 eV) in HTL and a low HOMO level (−6.8 eV) in

ETL.[56,57] Figure S11b presents a histogram of η_{CE} based on the fabricated 52 devices with the optimal conditions, exhibiting an average η_{CE} of 10.31 cd A^{-1}. A higher L_{max} of 4425 cd m^{-2} is further achieved by spin-coating the EML twice, but the efficiencies are slightly reduced. We also demonstrate high-efficiency 2D MAPbBr$_3$-based devices (η_{CE} = 8.43 cd A^{-1}, η_{PE} = 7.64 lm W^{-1}, η_{ext} = 2.06%, and L_{max} = 2735 cd m^{-2}) (Figures S12 and S13), as described in detail in the Supporting Information.

Finally, we demonstrate large-area and ultra-flexible LEDs based on the 2D FAPbBr$_3$ perovskites. Figure 4a presents the EL spectra of a large-area (3 cm^2) device under different driving voltages, showing emission wavelengths of 530 ± 1 nm and a
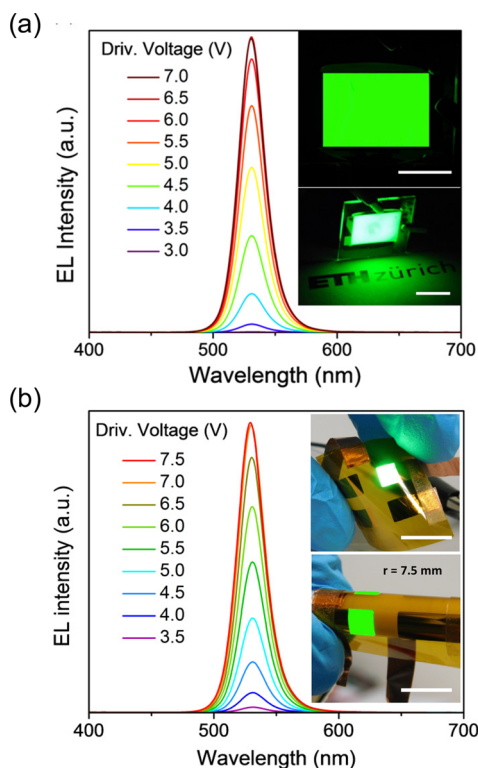
Figure 4. Demonstration of large-area and ultraflexible LEDs using FAPbBr$_3$ 2D perovskites. (a) EL spectra of a large-area (20 mm × 15 mm) LED at different driving voltages. Inset: Photographs of a large area device operating at 4.0 V (top) and 5.0 V (bottom). Logo reproduced with permission. Copyright 2017 ETH Zürich, Switzerland. (b) EL spectra of a flexible LED on the polyimide substrate at different driving voltages. Inset: Photographs of a flexible perovskite LED at different bending radii (scale bar: 1 cm).

fwhm of 22.6 nm, which are also consistent with the PL spectrum (Figure 2a). More importantly, with the optimized device architecture, the device performance does not compromise significantly (η_{CE} = 8.4 cd A^{-1}, η_{PE} = 6.6 lm W^{-1}, and η_{ext} = 2.0%) (Figure S14), and to our knowledge, it is the largest perovskite LED ever reported, with record high efficiency.[26,59] Figure 4b exhibits an ultra-flexible device on a thin polyimide substrate (50 μm). The insets show photographs of a working device under different degrees of bending. More details about device fabrication, characteristics, and bending tests can be found in section 3.2 and Figure S15 in the Supporting Information. Similarly, the EL spectra under different driving voltages are consistent and stable. Because of the ultra-flexible substrate considered here, a minimum bending radius down to 2 mm was achieved (Figure S15e). The turn-on voltage (V_{on}) for the flexible device is slightly higher due to a higher resistivity of the ITO layer deposited on the polyimide surface. The large-area, ultra-flexible devices demonstrated here give promise of the low-cost, large-scale production of the ultrapure green LEDs for the next generation of displays.

In summary, we demonstrate that in the colloidal 2D FAPbBr$_3$ perovskite system, one can introduce a small degree of quantum confinement that results in a proper bandgap and bandwidth for achieving the Rec. 2020 standard. In combination with its monodispersity in solution, the emission wavelength in the final LED devices is nearly identical to that in the diluted solution, clearly outperforming the OLED and QD technologies. Through the DQW and interface engineering, the LED devices exhibit ultrahigh color purity and high efficiency, which allow us to achieve the Rec. 2020 color coordinates for the first time. The results presented here open an avenue toward the realization of large-area, low-cost LEDs with an ultra-wide gamut. We believe that further optimization of device performance and the development of perovskite-based optoelectronics will be greatly facilitated by the original concepts proposed here.

■ ASSOCIATED CONTENT

ⓢ Supporting Information

The Supporting Information is available free of charge on the ACS Publications website at DOI: 10.1021/acs.nanolett.7b01544.

Additional details on synthetic procedures, characterization techniques and parameters, materials, fabrication, and characterization of perovskite LED devices. Supplementary figures including absorption and PL spectra of 2D perovskites, GIWAXS diffraction patterns, additional STEM images, temperature-dependent PL spectra, additional TRPL spectra, UPS spectra of 2D perovskites, molecular structures of other materials used in LEDs, AFM and SEM images for emissive layer, a cross-section SEM image of LED, device performance and architecture for small- and large-area devices, and photographs and EL characteristics of flexible perovskite LEDs. Tables showing comparative device performance. (PDF)

■ AUTHOR INFORMATION

Corresponding Author

*E-mail: chih-jen.shih@chem.ethz.ch. Phone: +41-44-633-42-40.

ORCID ⓘ

Sudhir Kumar: 0000-0002-2994-7084
Wendelin J. Stark: 0000-0002-8957-7687
Tae-Woo Lee: 0000-0002-6449-6725
Chih-Jen Shih: 0000-0002-5258-3485

Author Contributions

#S.K. and J.J. contributed equally to this work. S.K., J.J., and C.J.S. conceived and designed the experiments. S.K. designed, fabricated, and characterized the LED devices. J.J. synthesized and characterized the colloidal 2D perovskites. K.N. helped in LED fabrication, and F.J. helped with the colloidal 2D perovskite synthesis. Y.H.K. performed the TRPL and temperature-dependent PL measurement in the guidance of T.W.L. C.W. carried out the UPS analysis. Y.C.C. performed the GIXD analysis. S.K. and T.T. performed the AFM and SEM analysis. C.J.H performed the STEM analysis with the supervision of W.J.S. T.T. made the schematic device figure. S.K. and C.J.S. prepared all the graphics and co-wrote the paper. All authors discussed the results and commented on the manuscript.

Notes

The authors declare no competing financial interest.

■ ACKNOWLEDGMENTS

■ REFERENCES

(1) Pust, P.; Schmidt, P. J.; Schnick, W. *Nat. Mater.* **2015**, *14*, 454−458.

(2) Zhu, R.; Luo, Z.; Chen, H.; Dong, Y.; Wu, S.-T. *Opt. Express* **2015**, *23*, 23680−23693.

(3) Steckel, J. S.; Ho, J.; Coe-Sullivan, S. *Photonics Spectra* **2014**, *48* (9), 55−61.

(4) Shirasaki, Y.; Supran, G. J.; Bawendi, M. G.; Bulovic, V. *Nat. Photonics* **2012**, *7*, 13−23.

(5) Weidman, M. C.; Seitz, M.; Stranks, S. D.; Tisdale, W. A. *ACS Nano* **2016**, *10*, 7830−7839.

(6) Eperon, G. E.; Stranks, S. D.; Menelaou, C.; Johnston, M. B.; Herz, L. M.; Snaith, H. J. *Energy Environ. Sci.* **2014**, *7*, 982−988.

(7) Zhang, F.; Zhong, H. Z.; Chen, C.; Wu, X. G.; Hu, X. M.; Huang, H. L.; Han, J. B.; Zou, B. S.; Dong, Y. P. *ACS Nano* **2015**, *9*, 4533−4542.

(8) Kim, Y.-H.; Cho, H.; Lee, T.-W. *Proc. Natl. Acad. Sci. U. S. A.* **2016**, *113* (42), 11694−11702.

(9) Bade, S. G. R.; Li, J. Q.; Shan, X.; Ling, Y. C.; Tian, Y.; Dilbeck, T.; Besara, T.; Geske, T.; Gao, H. W.; Ma, B. W.; Hanson, K.; Siegrist, T.; Xu, C. Y.; Yu, Z. B. *ACS Nano* **2016**, *10*, 1795−1801.

(10) Milot, R. L.; Sutton, R. J.; Eperon, G. E.; Haghighirad, A. A.; Hardigree, J. M.; Miranda, L.; Snaith, H. J.; Johnston, M. B.; Herz, L. M. *Nano Lett.* **2016**, *16*, 7001−7007.

(11) Rehman, W.; Milot, R. L.; Eperon, G. E.; Wehrenfennig, C.; Boland, J. L.; Snaith, H. J.; Johnston, M. B.; Herz, L. M. *Adv. Mater.* **2015**, *27*, 7938−7944.

(12) Wehrenfennig, C.; Eperon, G. E.; Johnston, M. B.; Snaith, H. J.; Herz, L. M. *Adv. Mater.* **2014**, *26*, 1584−1589.

(13) Cho, H. C.; Jeong, S. H.; Park, M. H.; Kim, Y. H.; Wolf, C.; Lee, C. L.; Heo, J. H.; Sadhanala, A.; Myoung, N.; Yoo, S.; Im, S. H.; Friend, R. H.; Lee, T. W. *Science* **2015**, *350*, 1222−1225.

(14) Kim, Y.-H.; Cho, H.; Heo, J. H.; Kim, T.-S.; Myoung, N.; Lee, C.-L.; Im, S. H.; Lee, T.-W. *Adv. Mater.* **2015**, *27*, 1248−1254.

(15) Frost, J. M.; Walsh, A. *Acc. Chem. Res.* **2016**, *49*, 528−535.

(16) Pecchia, A.; Gentilini, D.; Rossi, D.; Auf der Maur, M.; Di Carlo, A. *Nano Lett.* **2016**, *16*, 988−992.

(17) Zhu, H.; Miyata, K.; Fu, Y.; Wang, J.; Joshi, P. P.; Niesner, D.; Williams, K. W.; Jin, S.; Zhu, X.-Y. *Science* **2016**, *353*, 1409−1413.

(18) Kim, H.-S.; Im, S. H.; Park, N.-G. *J. Phys. Chem. C* **2014**, *118*, 5615−5625.

(19) Green, M. A.; Ho-Baillie, A.; Snaith, H. J. *Nat. Photonics* **2014**, *8*, 506−514.

(20) Stranks, S. D.; Snaith, H. J. *Nat. Nanotechnol.* **2015**, *10*, 391−402.

(21) Sutherland, B. R.; Sargent, E. H. *Nat. Photonics* **2016**, *10*, 295−302.

(22) Tan, Z. K.; Moghaddam, R. S.; Lai, M. L.; Docampo, P.; Higler, R.; Deschler, F.; Price, M.; Sadhanala, A.; Pazos, L. M.; Credgington, D.; Hanusch, F.; Bein, T.; Snaith, H. J.; Friend, R. H. *Nat. Nanotechnol.* **2014**, *9*, 687−692.

(23) Wei, Z. H.; Perumal, A.; Su, R.; Sushant, S.; Xing, J.; Zhang, Q.; Tan, S. T.; Demir, H. V.; Xiong, Q. H. *Nanoscale* **2016**, *8*, 18021−18026.

(24) Li, G. R.; Rivarola, F. W. R.; Davis, N.; Bai, S.; Jellicoe, T. C.; de la Pena, F.; Hou, S. C.; Ducati, C.; Gao, F.; Friend, R. H.; Greenham, N. C.; Tan, Z. K. *Adv. Mater.* **2016**, *28*, 3528−3534.

(25) Li, J.; Xu, L.; Wang, T.; Song, J.; Chen, J.; Xue, J.; Dong, Y.; Cai, B.; Shan, Q.; Han, B.; Zeng, H. *Adv. Mater.* **2017**, *29*, 1603885.

(26) Wang, N. N.; Cheng, L.; Ge, R.; Zhang, S. T.; Miao, Y. F.; Zou, W.; Yi, C.; Sun, Y.; Cao, Y.; Yang, R.; Wei, Y. Q.; Guo, Q.; Ke, Y.; Yu, M. T.; Jin, Y. Z.; Liu, Y.; Ding, Q. Q.; Di, D. W.; Yang, L.; Xing, G. C.; Tian, H.; Jin, C. H.; Gao, F.; Friend, R. H.; Wang, J. P.; Huang, W. *Nat. Photonics* **2016**, *10*, 699−704.

(27) Xiao, Z.; Kerner, R. A.; Zhao, L.; Tran, N. L.; Lee, K. M.; Koh, T.-W.; Scholes, G. D.; Rand, B. P. *Nat. Photonics* **2017**, *11*, 108−115.

(28) Seo, H.-K.; Kim, H.; Lee, J.; Park, M.-H.; Jeong, S.-H.; Kim, Y.-H.; Kwon, S.-J.; Han, T.-H.; Yoo, S.; Lee, T.-W. *Adv. Mater.* **2017**, *29*, 1605587.

(29) Byun, J.; Cho, H.; Wolf, C.; Jang, M.; Sadhanala, A.; Friend, R. H.; Yang, H.; Lee, T.-W. *Adv. Mater.* **2016**, *28*, 7515−7520.

(30) Manser, J. S.; Christians, J. A.; Kamat, P. V. *Chem. Rev.* **2016**, *116*, 12956−13008.

(31) Li, G.; Rivarola, F. W. R.; Davis, N. J. L. K.; Bai, S.; Jellicoe, T. C.; de la Peña, F.; Hou, S.; Ducati, C.; Gao, F.; Friend, R. H.; Greenham, N. C.; Tan, Z.-K. *Adv. Mater.* **2016**, *28*, 3528−3534.

(32) Sadhanala, A.; Ahmad, S.; Zhao, B.; Giesbrecht, N.; Pearce, P. M.; Deschler, F.; Hoye, R. L. Z.; Gödel, K. C.; Bein, T.; Docampo, P.; Dutton, S. E.; De Volder, M. F. L.; Friend, R. H. *Nano Lett.* **2015**, *15*, 6095−6101.

(33) Koutselas, I. B.; Ducasse, L.; Papavassiliou, G. C. *J. Phys.: Condens. Matter* **1996**, *8*, 1217.

(34) Dou, L.; Wong, A. B.; Yu, Y.; Lai, M.; Kornienko, N.; Eaton, S. W.; Fu, A.; Bischak, C. G.; Ma, J.; Ding, T.; Ginsberg, N. S.; Wang, L.-W.; Alivisatos, A. P.; Yang, P. *Science* **2015**, *349*, 1518−1521.

(35) Sichert, J. A.; Tong, Y.; Mutz, N.; Vollmer, M.; Fischer, S.; Milowska, K. Z.; García Cortadella, R.; Nickel, B.; Cardenas-Daw, C.; Stolarczyk, J. K.; Urban, A. S.; Feldmann, J. *Nano Lett.* **2015**, *15*, 6521−6527.

(36) Bekenstein, Y.; Koscher, B. A.; Eaton, S. W.; Yang, P.; Alivisatos, A. P. *J. Am. Chem. Soc.* **2015**, *137*, 16008−16011.

(37) Akkerman, Q. A.; Motti, S. G.; Srimath Kandada, A. R.; Mosconi, E.; D'Innocenzo, V.; Bertoni, G.; Marras, S.; Kamino, B. A.; Miranda, L.; De Angelis, F.; Petrozza, A.; Prato, M.; Manna, L. *J. Am. Chem. Soc.* **2016**, *138*, 1010−1016.

(38) Vybornyi, O.; Yakunin, S.; Kovalenko, M. V. *Nanoscale* **2016**, *8*, 6278−6283.

(39) Quan, L. N.; Yuan, M.; Comin, R.; Voznyy, O.; Beauregard, E. M.; Hoogland, S.; Buin, A.; Kirmani, A. R.; Zhao, K.; Amassian, A.; Kim, D. H.; Sargent, E. H. *J. Am. Chem. Soc.* **2016**, *138*, 2649−2655.

(40) Bhaumik, S.; Veldhuis, S. A.; Ng, Y. F.; Li, M.; Muduli, S. K.; Sum, T. C.; Damodaran, B.; Mhaisalkar, S.; Mathews, N. *Chem. Commun.* **2016**, *52*, 7118−7121.

(41) Hassan, Y.; Song, Y.; Pensack, R. D.; Abdelrahman, A. I.; Kobayashi, Y.; Winnik, M. A.; Scholes, G. D. *Adv. Mater.* **2016**, *28*, 566−573.

(42) Kumar, S.; Jagielski, J.; Yakunin, S.; Rice, P.; Chiu, Y. C.; Wang, M.; Nedelcu, G.; Kim, Y.; Lin, S.; Santos, E. J.; Kovalenko, M. V.; Shih, C. J. *ACS Nano* **2016**, *10*, 9720−9729.

(43) Kojima, A.; Teshima, K.; Shirai, Y.; Miyasaka, T. *J. Am. Chem. Soc.* **2009**, *131*, 6050−6051.

(44) Liu, J. Y.; Xue, Y. Z.; Wang, Z. Y.; Xu, Z. Q.; Zheng, C. X.; Weber, B.; Song, J. C.; Wang, Y. S.; Lu, Y. R.; Zhang, Y. P.; Bao, Q. L. *ACS Nano* **2016**, *10*, 3536−3542.

(45) Meng, L.; Yao, E.-P.; Hong, Z.; Chen, H.; Sun, P.; Yang, Z.; Li, G.; Yang, Y. *Adv. Mater.* **2017**, *29*, 1603826.

(46) Ithurria, S.; Tessier, M. D.; Mahler, B.; Lobo, R. P. S. M.; Dubertret, B.; Efros, A. L. *Nat. Mater.* **2011**, *10*, 936−941.

(47) Galkowski, K.; Mitioglu, A.; Miyata, A.; Plochocka, P.; Portugall, O.; Eperon, G. E.; Wang, J. T.-W.; Stergiopoulos, T.; Stranks, S. D.; Snaith, H. J.; Nicholas, R. J. *Energy Environ. Sci.* **2016**, *9*, 962−970.

(48) Jeong, B. G.; Park, Y.-S.; Chang, J. H.; Cho, I.; Kim, J. K.; Kim, H.; Char, K.; Cho, J.; Klimov, V. I; Park, P.; Lee, D. C.; Bae, W. K. *ACS Nano* **2016**, *10*, 9297−9305.

(49) Jou, J. H.; Kumar, S.; Agrawal, A.; Li, T. H.; Sahoo, S. *J. Mater. Chem. C* **2015**, *3*, 2974−3002.

(50) Zhang, F. J.; Wang, S. J.; Wang, L.; Lin, Q. L.; Shen, H. B.; Cao, W. R.; Yang, C. C.; Wang, H. Z.; Yu, L.; Du, Z. L.; Xue, J. G.; Li, L. S. *Nanoscale* **2016**, *8*, 12182−12188.

(51) Yang, Y.; Zheng, Y.; Cao, W.; Titov, A.; Hyvonen, J.; Manders, J. R.; Xue, J.; Holloway, P. H.; Qian, L. *Nat. Photonics* **2015**, *9*, 259−266.

(52) Kathirgamanathan, P.; Kumaraverl, M.; Bushby, L. M.; Ravichandran, S.; Bramananthan, N.; Surendrakumar, S. *Dig. Tech. Pap. - Soc. Inf. Disp. Int. Symp.* **2016**, *47*, 652−656.

(53) Hu, H.; Salim, T.; Chen, B. B.; Lam, Y. M. *Sci. Rep.* **2016**, *6*, 33546.

(54) Kelly, G. *LED Magazine*, May 4, 2012, Part 2.

(55) Perumal, A.; Shendre, S.; Li, M. J.; Tay, Y. K. E.; Sharma, V. K.; Chen, S.; Wei, Z. H.; Liu, Q.; Gao, Y.; Buenconsejo, P. J. S.; Tan, S. T.; Gan, C. L.; Xiong, Q.; Sum, T. C.; Demir, H. V. *Sci. Rep.* **2016**, *6*, 36733.

(56) Tanaka, D.; Takeda, T.; Chiba, T.; Watanabe, S.; Kido, J. *Chem. Lett.* **2007**, *36*, 262−263.

(57) Kim, H. H.; Park, S.; Yi, Y.; Son, D. I.; Park, C.; Hwang, D. K.; Choi, W. K. *Sci. Rep.* **2015**, *5*, 8968.

(58) Thesen, M. W.; Höfer, B.; Debeaux, M.; Janietz, S.; Wedel, A.; Köhler, A.; Johannes, H.-H.; Krueger, H. *J. Polym. Sci., Part A: Polym. Chem.* **2010**, *48*, 3417−3430.

(59) Jagielski, J.; Kumar, S.; Yu, W.-Y.; Shih, C.-J. *J. Mater. Chem. C* **2017**, *5*, 5610−5627.